MDJ Cole et al.

Toroidal Alfven eigenmodes with nonlinear gyrokinetic and fluid hybrid models

Preprint of Paper to be submitted for publication in
Physics of Plasmas

Toroidal Alfvén eigenmodes with nonlinear gyrokinetic and fluid hybrid models

M D J Cole[1], A Biancalani[2], A Bottino[2], R. Kleiber[1], A Könies[1] and A Mishchenko[1]

[1] Max Planck Institue for Plasma Physics, D-17491 Greifswald, Germany
[2] Max Planck Institue for Plasma Physics, D-85748 Garching, Germany

E-mail: `michael.cole@ipp.mpg.de`

Abstract.
Alfvén eigenmodes may be important in driving fast particle transport in magnetic confinement fusion devices, with potentially deleterious results. To explain and predict this behaviour, numerical simulations are necessary. In order to predict transport, modes must be simulated through to their nonlinear saturated state. In this work, the first fully gyrokinetic self-consistent global simulations are performed that treat the nonlinear wave-particle interaction between fast particles and a single Toroidal Alfvén Eigenmode in a tokamak. It is shown that, in a standard benchmark case, two gyrokinetic codes produce consistent results. There is a polynomial relationship between the saturated perturbation level, $\delta B / B_0$, and the linear mode growth rate, γ_L, whose exponent reduces at higher γ_L. The fully gyrokinetic results are shown to qualitatively agree with those obtained using perturbative and non-perturbative hybrid models, the saturated perturbation level depending on the background damping.

1. Introduction

Alfvén eigenmodes are global electromagnetic modes, which exist in toroidal magnetic confinement fusion devices and can be driven unstable by fast particles created by heating and fusion. This can result in excessive transport of particles and energy which can, for example, cause damage to the device and therefore reduce its operational availability [1–3]. It is therefore important to understand and be able to predict these phenomena in order to avoid and mitigate them. Codes that numerically solve kinetic and fluid equations are the primary means of doing so.

Currently a number of codes are used to study Alfvén wave physics, implementing models of varying complexity and physical completeness. More complete models include more physical effects while, in general, simpler models are faster and less susceptible to numerical limitations on the parameter space that they can model. For instance, they can be less susceptible to numerical limitations such as the cancellation problem [4, 5]. The electromagnetic gyrokinetic model is one of the most complete, in which kinetic equations are solved for all plasma species with the fast gyromotion decoupled [6, 7]. Global electromagnetic eigenvalue codes such as LIGKA [8] have permitted detailed studies of linear Alfvén wave physics, but cannot be directly applied to nonlinear simulations.

Global gyrokinetic initial value codes such as GYGLES, EUTERPE [9, 10], and ORB5 [11] are more easily adapted for nonlinear simulations, but have historically suffered from the cancellation problem (see above), which limits simulations of modes of long wavelength and at higher plasma β. In this paper the results of the first nonlinear simulations of Alfvén waves obtained using the global electromagnetic gyrokinetic codes EUTERPE and ORB5 will be presented. EUTERPE is designed to perform 3D global simulations, e.g. in stellarator geometry. ORB5 is designed for axisymmetric simulations, and was extended to include electromagnetic effects in the framework of the NEMORB project [12, 13]. ORB5 and EUTERPE solve physically equivalent equations, formulated in different coordinate systems for different numerical properties.

In addition to the fully gyrokinetic models, hybrid models of varying complexity are possible. Typically either the bulk electron species, or the entire bulk plasma, is described by a fluid equation instead of by a kinetic equation. The energetic particle species, however, must be treated in a kinetic description as inverse Landau damping is the key mechanism for energetic particles to drive an Alfvén wave unstable. In addition to the choice of model for the bulk plasma, the mode may either be calculated independently of the influence of fast particles and fixed, called the perturbative description, or fast particles may be allowed to modify the structure of the mode, called the non-perturbative or self-consistent description. In this work, two hybrid models will be considered: FLU-EUTERPE, a non-perturbative fluid-electron, gyrokinetic bulk and fast-ion model [14, 15], and CKA-EUTERPE, a perturbative reduced ideal MHD bulk plasma, gyrokinetic fast ion model [16].

These hybrid approaches have been extensively exploited. Other examples of self-consistent fluid-electron, gyrokinetic ion codes include GEM, GTC, and XHMGC [17–19], while other examples of perturbative hybrid codes include NOVA-K, CAS3D-K, AE3D-K and VENUS-K [20–23]. These codes differ in the completeness of their MHD treatment of the bulk plasma, which can result in differing mode structure. All, however, calculate a mode frequency independent of fast particle effects and then a growth rate based on the power transfer between an applied gyrokinetic fast particle species and a fixed mode.

In this paper, a standard reference case is used to compare the results of the EUTERPE, ORB5, FLU-EUTERPE and CKA-EUTERPE models simulating the nonlinear wave-particle interaction between a single Toroidal Alfvén Eigenmode (TAE mode) and a fast particle population in tokamak geometry. In section 2, the mathematical details of the models will be set out. In section 3, the two gyrokinetic models will first be benchmarked, and then a full comparison will be made for all four models over a range of values of the TAE linear growth rate. The paper concludes in section 4.

2. Numerical models

As described in section 1, four models will be considered in this work: the fully gyrokinetic models of EUTERPE and ORB5, which are physically equivalent but formulated in different coordinate systems; the self-consistent fluid-electron hybrid model FLU-EUTERPE; and the perturbative reduced ideal MHD plasma, gyrokinetic fast ion hybrid model CKA-EUTERPE. EUTERPE and ORB5 solve a gyrokinetic equation for each particle species, combined with a quasi-neutrality and Ampére's law equation for calculating the self-consistent effects of the field

perturbations. EUTERPE's gyrokinetic equations are formulated in the 'mixed variables' formulation [24, 25], while the ORB5 equations are formulated in the 'canonical momentum' or $p_\parallel$ formulation [7]. FLU-EUTERPE drops the gyrokinetic equation for the electron species, instead solving a continuity equation for the evolution of the electron density and Ohm's law and pressure closure equations [15]. CKA-EUTERPE consists of two codes: the reduced ideal MHD eigenvalue code CKA solving the time-independent vorticity equation for the perturbed potentials, and gyrokinetic EUTERPE in the $p_\parallel$ formulation calculating power transfer with a fast ion species [16]. In this section these four models will be concisely described.

2.1. Full gyrokinetics - mixed variables (EUTERPE)

The nonlinear electromagnetic Particle-in-Cell (PIC) code EUTERPE solves the gyrokinetic Vlasov equation for arbitrary species in general 3D geometry [10],

$$\frac{\partial f_{1s}}{\partial t} + \dot{\vec{R}} \cdot \frac{\partial f_{1s}}{\partial \vec{R}} + \dot{v}_\parallel \frac{\partial f_{1s}}{\partial v_\parallel} = -\dot{\vec{R}}^{(1)} \cdot \frac{\partial F_{0s}}{\partial \vec{R}} - \dot{v}_\parallel^{(1)} \frac{\partial F_{0s}}{\partial v_\parallel}, \tag{1}$$

where the superscript (1) indicates the perturbed equations of motion - i.e. those including only terms first order in perturbed fields ϕ and $A_\parallel$ - and $s = i, e$, or f indicates the species. The distribution function is split into perturbed and unperturbed components, such that the total distribution function $f_s = F_{0s} + f_{1s}$. The background distribution functions, F_{0s}, are prescribed, so that solving equation (1) for f_{1s} gives all information needed to calculate the total distribution function at the next timestep. The unperturbed bulk plasma distribution functions, $F_{0i,e}$, are taken to be Maxwellian. For fast particle species other choices have been used, such as slowing down distribution functions, but will not be employed in this work.

In the mixed variables formulation [24, 25], the equations of motion $\dot{\vec{R}}$ and $\dot{v}_\parallel$ are

$$\dot{\vec{R}} = \left(v_\parallel - \frac{q}{m} \left\langle A_\parallel^{(h)} \right\rangle \right) \vec{b}^* + \tag{2}$$

$$\frac{1}{qB_\parallel^*} \vec{b} \times \left[\mu \nabla B + q \nabla \left\langle \phi - v_\parallel A_\parallel^{(s)} - v_\parallel A_\parallel^{(h)} \right\rangle \right]$$

$$\dot{v}_\parallel = -\frac{1}{m} \left[\mu \nabla B + q \nabla \left\langle \phi - v_\parallel A_\parallel^{(h)} \right\rangle \right] \cdot \vec{b}^* - \tag{3}$$

$$\frac{q}{m} \frac{\partial A_\parallel^{(s)}}{\partial t} - \frac{\mu}{m} \frac{\vec{b} \times \nabla B}{B_\parallel^*} \cdot \nabla \left\langle A_\parallel^{(h)} \right\rangle$$

where ϕ and $A_\parallel = A_\parallel^{(s)} + A_\parallel^{(h)}$ are the perturbed electrostatic vector potentials respectively, and μ is the magnetic moment. Parallel magnetic field perturbations are neglected. $B_\parallel^* = \vec{b} \cdot \nabla \times A_\parallel^*$, where $\vec{b}^* = \nabla \times \vec{A}^*$. $A^* = \vec{A}_0 + (mv_\parallel/q)\vec{b}$ is the modified vector potential and $\vec{A}_0$ is the background vector potential, such that $\vec{B}_0 = \nabla \times \vec{A}_0$. The background magnetic field unit vector $\vec{b} = \vec{B}/B$. The magnetic moment is defined as $\mu = mv_\perp^2/2B$. The gyroaverage operator is defined as

$$\langle z \rangle = \oint \frac{d\theta}{2\pi} z \left(\vec{R} + \vec{\rho} \right), \tag{4}$$

where z is a scalar field. The gyroaverage is numerically performed by an N-point fixed sum method.

Self-consistent electrostatic and parallel magnetic potentials are calculated using the quasi-neutrality equation in the long-wavelength approximation,

$$-\nabla \left[\left(\sum_{s=i,e,f} \frac{q_s^2 n_s}{T_s} \rho_s^2 \right) \nabla_\perp \phi \right] = \sum_{s=i,e,f} q_s n_{1s}, \tag{5}$$

and parallel Ampére's law,

$$\left(\sum_{s=i,e,f} \frac{\hat{\beta}_s}{\rho_s^2} - \nabla_\perp^2 \right) A_\parallel^{(h)} = \mu_0 \sum_{s=i,e,f} j_{\parallel 1s} + \nabla_\perp^2 A_\parallel^{(s)}. \tag{6}$$

Here the perturbed gyrocentre density $n_{1s}(\vec{x}) = \int d^6 Z f_{1s} \delta \left(\vec{R} + \vec{\rho} + \vec{x} \right)$ and the perturbed gyrocentre current $j_{\parallel 1s}(\vec{x}) = \int d^6 Z f_{1s} v_\parallel \delta \left(\vec{R} + \vec{\rho} + \vec{x} \right)$, where $d^6 Z = B_\parallel^* d\vec{R} dv_\parallel d\mu d\theta$ is the phase space volume, $\rho_s = \sqrt{m_s T_s}/eB$ is the thermal gyroradius and $\hat{\beta}_s = \mu_0 n_{0s} T_s / B^2$ is the EUTERPE normalised beta, corresponding to half the plasma species beta. Finite Larmor radius (FLR) effects are neglected for electrons, on account of the small size of the gyroradius. The background plasma densities are constrained by the quasi-neutrality equation, $\sum_s q_s n_{0s} = 0$.

The distribution function is defined in terms of markers as follows,

$$f_{1s} \left(\vec{R}, v_\parallel, \mu, t \right) = \sum_{\nu=1}^{N_p} w_\nu(t) \frac{1}{\mathcal{J}} \delta \left(\vec{R} - \vec{R}_\nu \right) \delta \left(v_\parallel - v_{\parallel\nu} \right) \delta \left(\mu - \mu_\nu \right), \tag{7}$$

where N_p is the number of markets, w_ν is the marker weight and $\mathcal{J}$ is the Jacobian. The fields ϕ and $A_\parallel^{(s,h)}$ are defined on a 3D grid in terms of finite elements,

$$\phi(\vec{x}) = \sum_{l=1}^{N_s} \phi_l \Lambda_l(\vec{x}) \qquad\qquad A_\parallel(\vec{x}) = \sum_{l=1}^{N_s} a_l \Lambda_l(\vec{x}), \tag{8}$$

where $\Lambda_l(\vec{x})$ are finite elements, N_s the number of finite elements, and ϕ_l and a_l are spline coefficients.

An equation is also necessary to distribute $A_\parallel$ between $A_\parallel^{(s,h)}$, which here is

$$\frac{\partial A_\parallel^{(s)}}{\partial t} + \vec{b} \cdot \nabla \phi = 0, \tag{9}$$

in analogy to the ideal MHD Ohm's law. For a case with small perturbed parallel electric field, therefore, $A_\parallel$ will be accumulated primarily in $A_\parallel^{(s)}$, with $A_\parallel^{(h)}$ small by comparison. Additionally, by invoking the pullback transformation for the distribution function, at each time step the accumulated $A_\parallel$ can be accumulated in $A_\parallel^{(s)}$ [25].

Note that although the equations of motion here are valid for linear simulations, a consistent derivation of nonlinear equations yields additional terms for $\dot{\vec{R}}$ and $\dot{v}_\parallel$ of higher order. All such terms are at least linear in $A_\parallel^{(h)}$, however, and so are vanishing for an ideal mode. In this work, we consider a mode that closely approximates the ideal MHD result, which is necessary for it to have been considered accurately by ideal perturbative codes [26]. In future work a derivation of the higher order nonlinear terms [27] will be followed by a fuller exploitation of the mixed variables formulation to treat also non-ideal modes in the nonlinear regime.

2.2. Full gyrokinetics - $p_\parallel$ formulation (ORB5)

The electromagnetic gyrokinetic equations implemented in the gyrokinetic code ORB5 are physically equivalent to those implemented in EUTERPE. However, the equations are solved in a different coordinate system such that the formulation of the equations of motion, quasi-neutrality equation, and Ampére's law equation is different. The $p_\parallel$ formulation is equivalent to the mixed variables formulation with $A_\parallel^{(s)} = 0$ at all times, meaning that equation 9 vanishes. The same Vlasov equation, equation (1), is solved, but in this formulation the equations of motion are

$$\dot{\vec{R}} = \left(v_\parallel - \frac{q}{m} \left\langle A_\parallel \right\rangle \right) \vec{b}^* + \frac{1}{qB_\parallel^*} \vec{b} \times \left[\mu \nabla B + q \nabla \left\langle \phi - v_\parallel A_\parallel \right\rangle \right] \tag{10}$$

$$\dot{v}_\parallel = -\frac{1}{m} \left[\mu \nabla B + q \nabla \left\langle \phi - v_\parallel A_\parallel \right\rangle \right] \cdot \vec{b}^*, \tag{11}$$

the quasi-neutrality equation is

$$-\nabla \cdot \frac{n_0 m_s}{B^2} \nabla_\perp \phi = \sum_{s=i,e,f} q_s n_{1s}, \tag{12}$$

and Ampére's law is

$$\left(\sum_{s=i,e,f} \frac{\hat{\beta}_s}{\rho_s^2} - \nabla_\perp^2 \right) A_\parallel = \mu_0 \sum_{s=i,e,f} j_{\parallel 1s}. \tag{13}$$

Numerically, a key difference between this formulation at the 'mixed variables' formulation described previously is the magnitude of the 'skin terms' proportional to $\frac{\hat{\beta}_s}{\rho_s^2}$ in Ampére's law. These terms are the origin of the cancellation problem, which scales with the plasma β and inversely with the species mass and $k_\perp \rho_i$. Whereas in the mixed variables formulation these terms are proportional to $A_\parallel^{(h)}$, which can be very small, in the $p_\parallel$ formulation these terms are proportional to the total perturbed vector potential $A_\parallel$. The cancellation problem is therefore often much more severe in the $p_\parallel$ formulation.

2.3. Fluid-electron hybrid model (FLU-EUTERPE)

The fluid-electron hybrid model couples the gyrokinetic Vlasov equation, with corresponding equations of motion, for the bulk ions and an optional fast ion species to a fluid equation for the evolution of the perturbed density of the electrons. This continuity equation is derived as a zeroth-order moment of the drift kinetic equation [14], yielding

$$\frac{\partial n_{1e}}{\partial t} + n_0 \vec{B} \cdot \nabla \left(\frac{u_{\parallel 1e}}{B} \right) + B \vec{v}_E \cdot \nabla \left(\frac{n_0}{B} \right) + \tag{14}$$

$$\left(\nabla \times A_\parallel \vec{b} \right) \cdot \nabla \left(\frac{n_0 u_{\parallel 0e}}{B} \right) +$$

$$n_0 \left(\vec{v}_* - \vec{v}_E \right) \cdot \frac{\nabla B}{B} + \frac{\nabla \times \vec{B}}{B^2} \cdot \left[n_0 \nabla \phi - \frac{\nabla P_{1e}}{e} \right] = 0$$

where

$$\vec{v}_E = \frac{\vec{b} \times \nabla \phi}{B}, \qquad\qquad \vec{v}_* = 2 \frac{\vec{b} \times \nabla P_{1e}}{n_0 e B}. \tag{15}$$

The equation for the perturbed electron pressure is

$$\frac{\partial P_{1e}}{\partial t} = -\vec{v}_E \cdot \nabla P_0 = -\frac{\vec{b} \times \nabla \phi}{B} \cdot \nabla n_0 T_0. \tag{16}$$

The perturbed vector potential is related to the electrostatic potential by an Ohm's law with optional resistivity term,

$$E_\| = -\nabla_\| \phi - \frac{\partial A_\|}{\partial t} = -\eta \nabla_\perp^2 A_\|, \tag{17}$$

where η parametises the resistivity.

The fluid and gyrokinetic species are related by Ampére's law,

$$e n_0 u_{\|1e} = \sum_{s=i,f} j_{\|s} + \frac{1}{\mu_0} \nabla_\perp^2 A_\| \tag{18}$$

and the quasi-neutraliy equation, where $u_{\|1e}$ and n_{1e} are fields discretised on the grid, while $j_{\|1i}$ and n_{1i} are quantities discretised with markers.

2.4. Perturbative reduced ideal MHD hybrid (CKA-EUTERPE)

CKA-EUTERPE is a perturbative hybrid code package. The reduced ideal MHD eigenvalue code CKA calculates an eigenfunction by solving the vorticity equation,

$$\omega^2 \nabla \cdot \left(\frac{1}{v_A^2} \nabla_\perp \phi \right) + \nabla \cdot \left[\vec{b} \nabla_\perp^2 \left(\vec{b} \cdot \nabla \right) \phi \right] + \nabla \cdot \left[\vec{b} \nabla \cdot \left(\frac{\mu_0 j_{\|1}}{B} \vec{b} \times \nabla \phi \right) \right]$$

$$- \nabla \cdot \left(\frac{2\mu_0}{B^2} \left[\left(\vec{b} \times \nabla \phi \right) \cdot \nabla P_1 \right] \left(\vec{b} \times \kappa \right) \right) = 0, \tag{19}$$

to yield the perturbed electrostatic potential, ϕ. The curvature tensor, κ, is defined as

$$\vec{\kappa} = \vec{b} \cdot \nabla \vec{b} = \left(\nabla \times \vec{b} \right) \times \vec{b} \tag{20}$$

Note that the Fourier transform $\phi(s,t) = \phi(s) e^{-i\omega t}$ has been applied to eliminate the time derivative. CKA is an eigenvalue code solving a time-independent problem. CKA therefore yields a reduced ideal MHD real frequency, in addition to the time-independent mode structure without the influence of fast particles. These are then passed to the gyrokinetic code EUTERPE, which models a species of fast ions in order to calculate the power transfer to or from the mode.

3. Numerical results

In this section we consider the nonlinear physics of the ITPA toroidal Alfvén eigenmode (TAE) benchmark case [26, 28]. The magnetic equilibrium is that of a large aspect ratio circular tokamak, with major radius $R_0 = 10.0$ m and minor radius $r_a = 1.0$ m. The magnetic field strength on axis $B_0 = 3.0$ T, and the safety factor profile is given by the equation $q(r) = 1.71 + 0.16 (r/a_0)^2$. The bulk plasma density and temperature profiles are flat, with a background density $n_0 = 2 \times 10^{19}$ m^{-3} and temperatures $T_i = T_e = 1$ keV. The bulk ion species is hydrogen.

In figure 1, the resulting Alfvén continuum is plotted for mode numbers $n = -6$ and $m = 10, 11$. A toroidicity gap is visible centred at $s = 0.25$ (note that, for circular flux surfaces, $s = r^2$). The ITPA TAE benchmark case concerns this single mode.
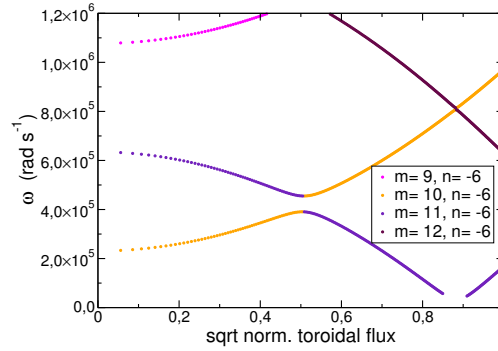
Figure 1. The continuum for the ITPA toroidal Alfvén eigenmode benchmark case, around the $n = -6$, $m = 10, 11$ toroidicity gap [26, 28].

A fast minority deuterium species is applied with a density given by the equation

$$n_f(r) = n_{0f} \exp\left(-c_1 \tanh\left(\frac{r - c_2}{c_3}\right)\right) \tag{21}$$

where $n_{0f} = 7.51352 \times 10^{16}$ m^{-3}, $c_1 = 0.666400$, $c_2 = 0.49123$ and $c_3 = 0.198739$. The fast particle distribution function is Maxwellian with the temperature fixed at $T_f = 400$ keV except where explicitly stated otherwise. This is the fast particle temperature at which the linear growth rate is a maximum given the other parameters. In all simulations Dirichlet boundary conditions are applied at the axis and at the edge.

Nonlinearly we expect the behaviour of the mode to divide into at least two distinct stages. In the first, linear stage, the amplitude of the perturbed potentials is small relative to the background fields. The nonlinear terms proportional to ϕf_{1s} and $A_\parallel f_{1s}$ are correspondingly small, and the behaviour of the mode does not differ substantially to the linear treatment in [26]. In the second, nonlinear stage, the nonlinear terms become comparable in magnitude to the linear terms, and should produce a saturation in the mode amplitude.

In this paper only the wave-particle nonlinearity is considered. This means that the nonlinear Vlasov equation, equation 1, is solved only for the fast particle species, $s = f$. For the bulk species $s = i, e$, the linearised Vlasov equation

$$\frac{\partial f_{1s}}{\partial t} + \dot{\vec{R}}^{(0)} \cdot \frac{\partial f_{1s}}{\partial \vec{R}} + \dot{v}_\parallel^{(0)} \frac{\partial f_{1s}}{\partial v_\parallel} = -\dot{\vec{R}}^{(1)} \cdot \frac{\partial F_{0s}}{\partial \vec{R}} - \dot{v}_\parallel^{(1)} \frac{\partial F_{0s}}{\partial v_\parallel}, \tag{22}$$

is solved instead, where $\dot{\vec{R}}^{(0)}$ and $\dot{v}_\parallel^{(0)}$ correspond to the equations of motion excluding terms proportional to the perturbed fields ϕ and $A_\parallel$.

3.1. Gyrokinetic validation

In this section the numerical solution of the gyrokinetic equations for the ITPA TAE case is compared using the EUTERPE and ORB5 codes. There is a discrepancy between the linear growth rates calculated using each code [13, 26]. This discrepancy may be due to e.g. differences in the discretisation of the numerical equilibrium, or in the different normalization of the fast-particle density profile. As it is known that the nonlinear physics is parameterised by the linear growth rate, for the nonlinear
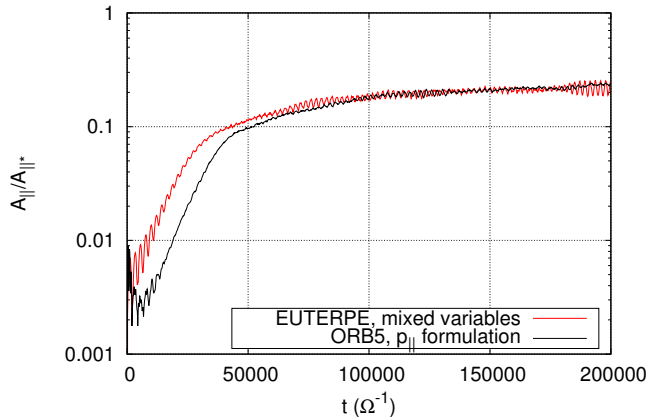
Figure 2. The evolution of the perturbed parallel vector potential in EUTERPE-ORB5 normalised units, $A_{\parallel *}$, plotted for EUTERPE solving the gyrokinetic Vlasov-Maxwell equations in the mixed variables formulation and ORB5 solving the same system of equations in the $p_\parallel$ formulation. Note the close agreement in saturated amplitude despite differing initial amplitudes.

benchmark these linear differences are normalised by adjusting the fast particle concentrations such that the linear growth rate is equal in both codes.

The ITPA TAE parameters are taken with $T_f = 500$ keV. The fast particle concentration used in EUTERPE is reduced by a factor 0.3, such that the same linear growth rate $\gamma_L = 3.5 \times 10^4$ rads^{-1} is calculated by both codes. Only the wave-particle nonlinearity is considerd here, so the linear Vlasov equation is solved for bulk ions and electrons, while the nonlinear Vlasov equation is solved for fast ions.

In figure 2, the normalised perturbed parallel vector potential, $A_{\parallel *}$, is plotted for both codes. This is defined as $A_{\parallel *} = B_* r_*$, where B_* is the magnetic field strength at the magnetic axis, $r_* = \frac{\sqrt{k_B T_* m_p}}{|e| B_*}$, and $T_* = T_e(s = 0.5)$. Good agreement is seen, giving grounds for confidence in the nonlinear gyrokinetic approach, although differences may be present due to differences in treatment of the linear physics by the two codes.

3.2. Model comparison and saturation level scaling

Having established the validity of the gyrokinetic approach, we consider the case with an additional two models: the nonlinear fluid-electron hybrid model FLU-EUTERPE with and without resistive damping, and the perturbative hybrid model CKA-EUTERPE. In all cases, nonlinear terms have only been considered in solving the gyrokinetic Vlasov equation for the energetic particle population, which is taken to have a temperature $T_f = 400$ keV. The difference, as detailed in section 2, is in the completeness of treatment of the bulk plasma. Non-linear simulations in this section have been performed with a reduced mass ratio of $m_e/m_i = 0.005$ in used in order to reduce computational requirements; simulations with realistic mass ratio have been performed for the nominal ITPA parameters and do not show a significant difference.

In table 1, the computational requirements of ORB5, and each model in the EUTERPE code package, for the ITPA TAE benchmark case in the linear regime are

Model	Markers	Timestep	CPU-hrs (to $10^5 \Omega_c^{-1}$)
CKA-EUTERPE	8×10^5	20.0	6
FLU-EUTERPE	2×10^5	10.0	18
EUTERPE ($p_\parallel$)	3×10^7	0.75	80000
EUTERPE (mixed)	3×10^6	10.0	256
ORB5 ($p_\parallel$)	3×10^7	5.0	22000

Table 1. A table depicting the computational requirements of each model for the linear ITPA TAE case with nominal parameters to reach an 'end time' of $10^5 \ \Omega_c^{-1}$, at which all the properties of interest of the mode are well established and can by diagnosed with good accuracy.

detailed. The computational requirements of nonlinear simulations are greater, but proportional to those of the linear simulations, increased primarily by the need for higher toroidal resolution. Both the hybrid models and the mixed variables gyrokinetic scheme offer significant improvements over the gyrokinetic model in $p_\parallel$ formulation. The mixed variables formulation provides a two order of magnitude reduction in required CPU-hours for this case the fluid-electron hybrid model provides a further order of magnitude reduction.

A key quantity is the amplitude at which the magnetic field perturbation saturates nonlinearly. In figure 3, the maximum value of $\delta B/B_0$ in the simulation domain is plotted as it evolves in time for the gyrokinetic and fluid-electron hybrid EUTERPE models. Distinct linear growth and nonlinear saturation stages are visible. In both the fully gyrokinetic and the fluid-electron hybrid model without resistive damping the nonlinear stage begins at the same saturated amplitude level, order $\delta B/B_0 = 10^{-3}$. This is consistent with previous numerical work and is in order of magnitude agreement with observed experimental values [29], although it should be noted that the device parameters considered here are far from experiment.

The undamped fluid-electron hybrid model, however, exhibits a sub-exponential upward drift in $\delta B/B_0$, after the onset of the nonlinear stage and before a clear saturated amplitude is reached. This is a known feature of the perturbative hybrid approach. The presence of additional physical damping mechanisms in the more complete models may be the reason for the reduction in drift. The fully gyrokinetic model exhibits some oscillation in the solution, depicted in figure 4, which creates some uncertainty in the exact quantitative saturated perturbation amplitude.

Drift and oscillation is substantially eliminated in the fluid-electron hybrid model by the application of finite resistive damping (blue). Here a resistivity corresponding to a Lundquist number of order 10^4 is considered. However, finite resistivity also reduces the saturated perturbation amplitude to order 10% of the undamped value. The need to apply an unphysically strong damping to obtain a clear result is a drawback of this approach.

In previous work performed with the nonlinear kinetic-MHD perturbative hybrid code package CKA-EUTERPE [16, 30], the relationship between the linear growth rate γ_L of the TAE and the saturated amplitude of the magnetic field perturbation was considered. Taking otherwise the same physical and numerical parameters as earlier in this section, the linear growth rate is varied by scaling the fast particle concentration by a factor between 0.5 and 2.0. The linear growth rate can also be altered by removing finite Larmor radius (FLR) effects.
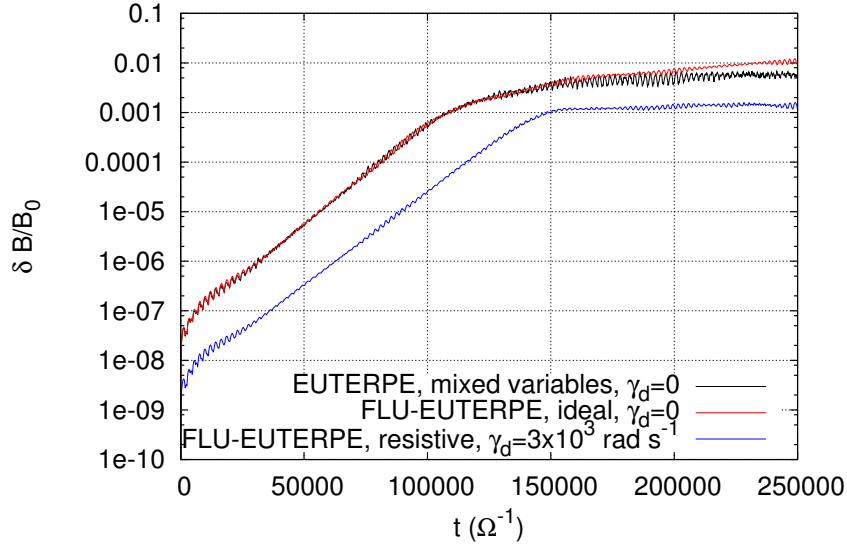
Figure 3. Evolution of the perturbed magnetic potential for EUTERPE models of decreasing complexity: fully gyrokinetic (black) and fluid-electron hybrid model with (blue) and without (red) resistive damping. Note that resistive damping strongly affects the saturated amplitude.
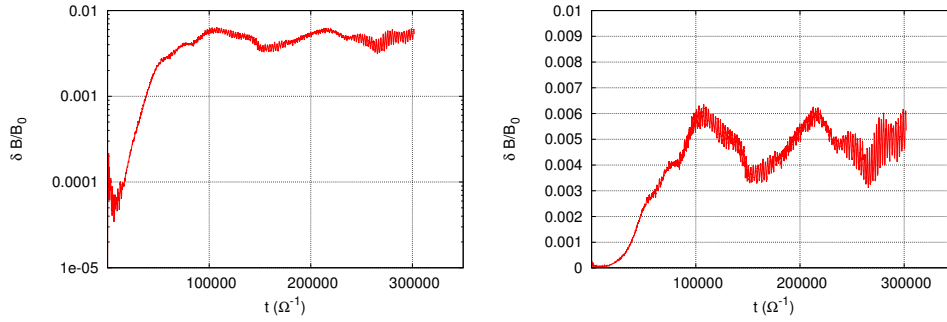

Figure 4. Comparison of the evolution of the maximum of the ratio of the perturbed magnetic potential to the background magnetic field, plotted on logarithmic (left) and linear (right) scales, from ORB5. Note there is significant oscillation in the solution.

In figure 5, the relationship between $\delta B/B_0$ at saturation and γ_L is plotted for three models: the fully gyrokinetic model (in mixed variables and $p_\parallel$ formulations), the fluid-electron hybrid model with resistive damping, and CKA-EUTERPE with ad-hoc damping. The fluid-electron hybrid model results are plotted with and without consideration of FLR effects.

In the case of fluid-electron hybrid simulations without damping, often no clear saturated amplitude is obtained, with the perturbation continuing to increase sub-exponentially for large time. In the fully gyrokinetic model, there is some ambiguity in the saturated level to be obtained. In this case, all values have been taken early
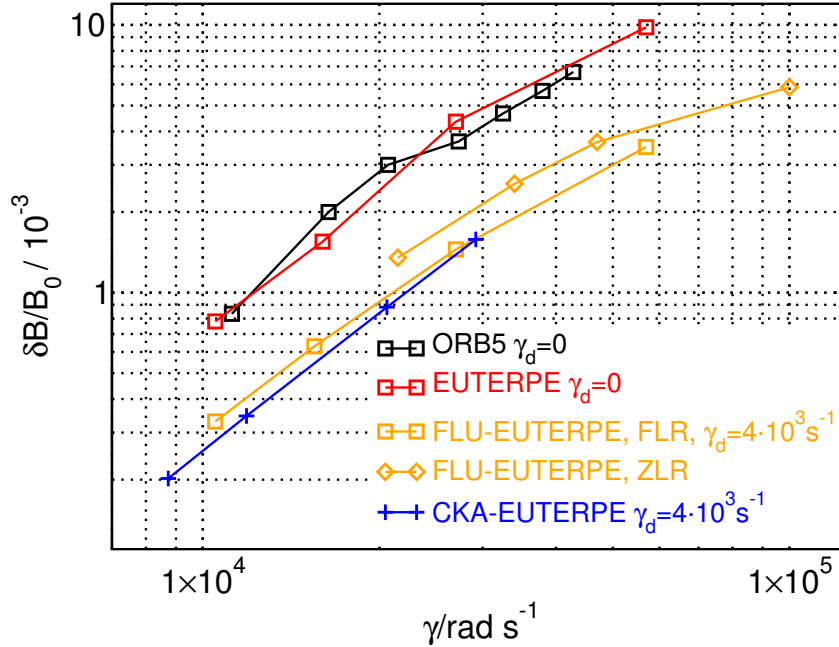
Figure 5. Linear growth rate γ_L plotted against saturated perturbation amplitude $\delta B/B_0$ for the nonlinear $m = 10, 11$, $n = -6$ ITPA TAE case plotted for perturbative hybrid model FLU-EUTERPE with (FLR) and without (ZLR) finite Larmor radius effects, and fully gyrokinetic codes EUTERPE and ORB5. The absolute amplitude is influenced by strength of applied damping, but the qualitative relationship is the same. Here the χ (toroidal) component of $\delta B/B_0$ is plotted; the total $\delta B/B_0$ is of the same order of magnitude.

in the saturated phase before the onset of any sub-exponential drift, an average being taken after the first inflection point following saturation.

All three models show qualitatively the same trend, with a divergence in level between those models with (fluid-electron hybrid, perturbative hybrid) and without (fully gyrokinetic) additional damping mechanisms. The inferred damping rate γ_d as $n_f \rightarrow 0$ is equalised for the fluid-electron and perturbative hybrid models at $\gamma_d = 4 \times 10^3$ rad s^{-1}. Note however that the implementation of damping differs between the two models, with the resistive damping of the fluid-electron hybrid model entering through a finite $E_\parallel$, while the ad-hoc damping implemented in the perturbative hybrid model retains an ideal MHD Ohm's law. In figure 6, the saturated amplitude is plotted for varying applied damping rates γ_d. For the perturbative hybrid model CKA-EUTERPE, the saturated amplitude diverges at low γ_d.

Without FLR effects, the fluid-electron hybrid model results exhibit the same qualitative trend but with a consistently higher saturated amplitude. This may be due at least in part to a reduction in damping by the bulk ions. Any influence of kinetic bulk ion effects is not present in the perturbative hybrid model CKA-EUTERPE.

The two fully gyrokinetic models exhibit the same trend at a higher level due to the absence of artificial damping. The two gyrokinetic codes show good quantitative agreement with one another. It is however significant that the agreement is not quantitatively as close as that seen in the direct comparison for a single case in figure 2,
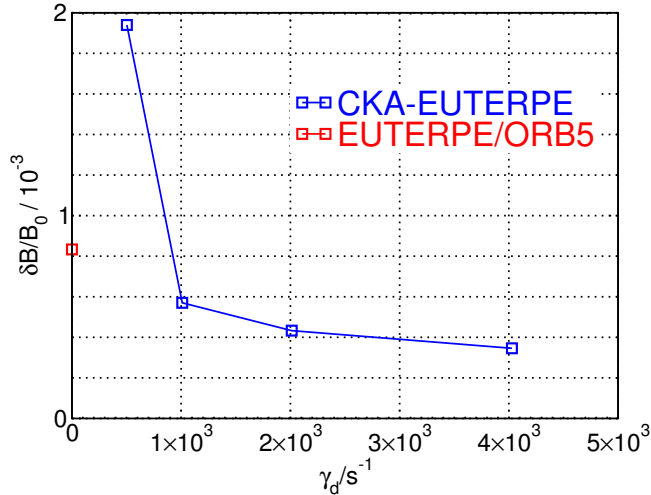
Figure 6. The variation of the saturated perturbation amplitude for the $T_f = 400$ keV case with different levels of applied damping, γ_d. Fast particle concentration is varied to ensure a constant γ_L. The perturbative hybrid model CKA-EUTERPE diverges significantly at low γ_d.

due to the uncertainty in the time at which to measure the saturated field perturbation amplitude.

4. Conclusion

In previous work a simple case has been considered in which a toroidal Alfvén eigenmode is driven linearly unstable via inverse Landau damping by fast particles. This case has been considered with a number of numerical tools, including fully gyrokinetic and fluid-kinetic hybrid models of varying completeness [26, 28]. In subsequent work, this case has also been considered nonlinearly with hybrid tools, such as the perturbative hybrid model CKA-EUTERPE, described in section 2.4 of this paper. In this work, simulations have been performed using a hierarchy of models including fully gyrokinetic, resistive and ideal non-perturbative fluid-electron hybrid, and perturbative reduced ideal MHD-kinetic hybrid.

The fully gyrokinetic simulations, performed nonlinearly for electromagnetic global modes for the first time, have been successfully benchmarked between two codes, EUTERPE and ORB5. The relationship between the linear growth rate of the mode, γ_L, and saturated magnetic field perturbation, $\delta B/B_0$, has been studied. With all models a polynomial relation (i.e. log-log linear) between γ_L and $\delta B/B_0$ is observed, where $\delta B/B_0$ increases with increasing γ_L. When γ_L is increased above 10^5 rad s^{-1} growth in $\delta B/B_0$ with γ_L weakens.

All models exhibit the same qualitative relationship between γ_L and $\delta B/B_0$. The absolute level of the saturated perturbation amplitude, however, is determined by the linear damping level. In the hybrid models, some artificial damping is required in order to obtain a stable saturated perturbation level. The absolute level of the saturated perturbation is therefore lower for these models than for the fully gyrokinetic model, in which physical and numerical damping suffices to obtain a measurable saturated

level. The neglect of bulk and fast ion FLR effects is shown to increase the saturated perturbation level at fixed γ_L, but does not alter the qualitative relationship between $\delta B / B_0$ and γ_L.

These results suggest that damping due to the bulk plasma has little qualitative influence on the nonlinear physics of a single TAE mode, but correctly modelling such damping is important in obtaining an accurate quantitative result for the saturated perturbed amplitude. That physical processes in the fully gyrokinetic models are able to replace an ad-hoc applied damping in the fluid-kinetic hybrid models is a clear advantage of the more complete treatment.

Having established the validity of these models in a simple case, and identified fundamental physical characteristics of such a system, in future work the nonlinear interaction of multiple modes and zonal structures through the bulk plasma can be considered using both the fully gyrokinetic and the fluid-electron hybrid models. Ultimately, a realistic treatment of collisions would allow the resistive damping to be considered self-consistently, which we propose is important for quantifying transport.

In this paper, a single mode benchmark case has been considered. Nonlinear interaction between multiple modes is, however, expected to be significant in predicting transport. Modes can interact through nonlinear modification of the fast particle profile, which influence drive and saturation. They can also interact directly via nonlinear terms in the Vlasov equations for the bulk ions and/or electron species. Preliminary work using EUTERPE and ORB5 suggests that the inclusion of multimode effects tends to reduce the calculated saturated perturbation amplitude. This broad subject will be addressed in greater detail in subsequent publications.

Finally, the $p_\parallel$ [7] and mixed variables [25] formulations of the gyrokinetic equations of motion have been benchmarked nonlinearly in this case and the mixed variables formulation shows a substantial reduction in required computational resources. It is believed that in a case where finite $E_\parallel$ effects are important, extended mixed variables equations including higher order terms must be solved [27]. This will be considered in future work.

Acknowledgments

References

[1] A. Fasoli *et al.*, Nucl. Fusion **47**, (2007).
[2] C. Z. Cheng, L. Chen, and M. S. Chance, Ann. Phys. **161**, 21 (1985).
[3] L. Chen and F. Zonca, Nucl. Fusion **47**, S727 (2007).
[4] R. Hatzky, A. Könies, and A. Mishchenko, Proceedings of the Joint Varenna-Lausanne International Workshop 13 (2004).
[5] R. Hatzky, A. Könies, and A. Mishchenko, J. Comp. Phys. **225**, 568 (2007).
[6] E. A. Frieman and L. Chen, Phys. Fluids **25**, 502 (1982).
[7] A. J. Brizard and T. S. Hahm, Rev. Mod. Phys. **79**, 421 (2007).
[8] P. Lauber, S. Günter, A. Könies, and S. D. Pinches, J. Comput. Physics **226**, 447 (2007).
[9] G. Jost *et al.*, Phys. Plasmas **8**, 3321 (2001).
[10] V. Kornilov *et al.*, Phys. Plasmas **11**, 3196 (2004).
[11] S. Jolliet *et al.*, Comput. Phys. Commun. **117**, 409 (2007).
[12] A. Bottino and E. Sonnendrücker, J. Plasma Phys. **81**, 435810501 (2015).
[13] A. Biancalani *et al.*, Phys. Plasmas **23**, 012108 (2016).
[14] M. D. J. Cole *et al.*, Phys. Plasmas **21**, 072123 (2014).
[15] M. D. J. Cole *et al.*, Plasma Phys. Control. Fusion **57**, 054013 (2015).
[16] T. Fehér, *Simulation of the interaction between Alfvén waves and fast particles* (Universität Greifswald, Germany, 2014).
[17] Y. Chen and S. Parker, Phys. Plasmas **8**, 441 (2000).
[18] Z. Lin and L. Chen, Phys. Plasmas **8**, 1447 (2001).
[19] X. Wang *et al.*, Phys. Plasmas **18**, 052504 (2011).
[20] N. N. Gorelenkov, C. Z. Cheng, and G. Y. Fu, J. Comput. Physics **6**, 2802 (1999).
[21] A. Könies, A. Mishchenko, and R. Hatzky, Theory of Fusion Plasmas 133 (2008).
[22] D. Spong, E. D'Azevedo, and Y. Todo, Contr. Plasma Phys. **50**, 708 (2010).
[23] W. A. Cooper, Plasma Phys. Control. Fusion **53**, 024001 (2011).
[24] A. Mishchenko, M. Cole, R. Kleiber, and A. Könies, Phys. Plasmas **21**, 052113 (2014).
[25] A. Mishchenko, A. Könies, R. Kleiber, and M. Cole, Phys. Plasmas **21**, 092110 (2014).
[26] A. Könies *et al.*, Proceedings of the 24th IAEA Fusion Energy Conference ITR/P1 (2012).
[27] R. Kleiber, A. Mishchenko, A. Könies, and R. Hatzky, Phys. Plasmas (accepted) (2016).
[28] A. Mishchenko, A. Könies, and R. Hatzky, Phys. Plasmas **16**, 082105 (2009).
[29] Y. Todo, M. A. V. Zeeland, A. Bierwage, and W. W. Heidbrink, Nucl. Fusion **54**, 4012 (2014).
[30] A. Könies *et al.*, In preparation .